5

Atomistic-Continuum Modelling of Coupled Fields and Defects in Semiconductor Crystals

Grzegorz Jurczak, Marcin Maździarz and Paweł Dłużewski

Institute of Fundamental Technological Research Polish Academy of Sciences
Warszawa, Poland
gjurcz@ippt.pan.pl, mmazdz@ippt.pan.pl, pdluzew@ippt.pan.pl

Abstract: The aim of this paper is to briefly present common procedures used for the atomic reconstruction of crystal structure affected by defects and its further atomistic–continuum modelling. From the theoretical point of view, the methodology presented here applies the continuum theory of dislocations and linear or nonlinear theory of elasticity. To solve a boundary-value problem for the semiconductor crystals with defects the finite element analysis is used. Except classical analytical solution based on the linear theory of dislocations proposed by Love [21], a more recent numerical method based on iterative approach for reconstruction of the atomic structure is discussed. It allows to enhance the accuracy of the atomistic configuration of selected defects against the classical

solution. In this paper, the attention is focused on the mechanical aspects of crystal defects modelling. This concerns the nonlinear effects of dislocation behaviour, as well as the configuration changes. Additionally, an alternative strain measure effect on the residual stresses is considered. Except theoretical approach to the modelling, experimental measurements of crystals affected by dislocations are applied. Computer processing of HRTEM images is used to measure and simulate crystal defects. Finally, the combination of the elastic and electric fields in quantum dot grown at the edge of threading dislocation is presented as an example of the coupled fields problem in semiconducting heterostructure. The content of this paper does not completely cover a subject, but rather represents an introduction and discusses a selected part of the literature for further studies in the subject.

Keywords: elasticity, dislocation, dislocation core, semiconductors.

5.1. Introduction

The very beginning of crystal plasticity based on dislocation concept can be found in works by Taylor [1], Orowan [2], and Polanyi [3]. Dislocations and dislocation loops initially introduced to explain the mechanism of crystal plasticity [4] turned out to be not only a purely mechanical object. Various types of defects and their related short or long-range elastic and electric fields play now an important role in the prediction of various physical properties of the crystal structure. It became evident shortly after the invention of the first transistor by Shockley and coworkers in Bell Laboratories. Very soon, many researchers discovered that the dislocations significantly modify the electrical properties of semiconducting crystals used in electronics [5, 6]. This also concerns short-wavelength light emitting devices (LED,LD) [7, 8] which have attracted attention for many years due to adjustable direct band gap, which allows us to cover a wide wavelength range from ultraviolet to near infrared. Threading Dislocation (TD), which is a common defect of semiconducting heterostructures, unavoidably arises in the layers during the growth process. Such defects, except local lattice disturbance, also compose non-radiative recombination centers [9, 10], which affects the efficiency and lifetime of optoelectronic devices. Emission spectra, which is another important parameter of the optoelectronic device, depend on the formation energy of dislocation core related to the atomic configuration [11, 12, 13]. Generally, the presence of dislocations in semiconducting crystals has a detrimental effect on the device quality, but then again some optimists claim that dislocations in semiconductors might exhibit unusual electrical properties, e.g. superconductivity along dislocation lines. More comprehensive history of the research related to dislocations in the semiconductors can be found in e.g. [14]

Despite intensive studies on semiconducting heterostructures, some interaction between the crystal defects and physical properties of semiconducting heterostructures is still subject of controversy. Furthermore, dislo- cations still are a technological

barrier for higher efficiency and durability of such materials in electronic and optoelectronic applications. Experimental measurements in this domain, based mainly on the Transmission Electron Microscopy (TEM) techniques, e.g. High Resolution TEM (HRTEM), Electron Energy Loss Spectroscopy (EELS), energy dispersive X-ray spectroscopy (EDS), etc. provide analytical and quantitative elucidation of nanostructural properties of crystals at the atomic level [15, 16, 17]. TEM techniques provide the possibility for a quantitative measurement with a very high accuracy, e.g. HRTEM allows reaching 0.03Å accuracy in displacement measurements [18]. However, because of the TEM measurements specific character, they are very toilsome. The TEM sample preparation, usually by ion milling, mechanically modifies the sample and many dislocations annihilate at the sample boundary, which makes the analysis very tricky. Additionally, during TEM observations the electron beam itself may be a source of compositional fluctuations and clustering [20]. Therefore, atomistic simulations have become a popular way to investigate the effect of crystal defects on the physical properties of heterostructures. It is well known that real crystals demonstrate an anisotropic behaviour, however, currently the most popular analytical approach to the dislocation core analysis is based on Love's equations [21] and its various modifications [4, 22, 23] and covers only the isotropic continuum. Fully anisotropic solutions, e.g. [24], due to more complex formulae, are not very popular. Such situation leads to the simulation of inaccurate atomistic configurations of adefected structure and may make results interpretation difficult or even incorrect. Here, among others, a relatively simple iterative procedure within the framework of the finite deformation theory is presented to improve the quality of the dislocation core configuration. This approach, which has classical Love's solution as a starting configuration, improves the accuracy of the reconstruction of the dislocation core.

This paper is organised as follows. Sections 2-3 describe the theoretical background and mathematical foundations for atomistic reconstruction of defected crystal structures. Next sections (4-5) describe an application of the methodology to the dislocations networks and the idea of an iterative algorithm based on the nonlinear approach. Section 6 describes an elastic and electric interaction of the threading dislocation and quantum dot (QD). Finally, in Section 7 a short discussion of the results is given and perspectives are presented.

5.2. Continuum Theory of Dislocations

In the classical continuum theory of elasticity the gradient of displacement vector, which describes deformation of the body, can be decomposed additively into symmetric small strain tensor ε and antisymmetric rotation tensor **w**,

$$\nabla \mathbf{u} = e + \mathbf{w} = \beta \tag{1}$$

In the continuum theory of dislocations, except elastic distortions β, some plastic

(also called source or initial) deformation arises, related to local lattice incompatibilities present in the crystal structure containing defects. Similarly to previous equation, we may use the following decomposition of the total displacement gradient

$$\nabla \mathbf{u}_{tot} = \underbrace{e + \mathbf{w}}_{\beta = \nabla \mathbf{u}} = \beta_{pl} \tag{2}$$

where β_{pl} denotes an asymmetric tensor of plastic distortion related to local and permanent rearrangement of the crystal configuration. In the continuum theory of dislocations, two complementary approaches to crystal defects with a slightly different notation are used, namely

- **in the continuum theory of discrete dislocations** it is assumed that the continuum composes a multiply connected region with discrete dislocations. After cutting off along slip planes such a region is treated as a single connected region for which the lattice displacement field reads $\mathbf{u}(\mathbf{x}) \neq \mathbf{u}_{tot}(\mathbf{x})$, and the lattice distortion is defined in a similar way as in the classical theory of elasticity

$$\beta \overset{df}{=} \nabla \mathbf{u} = e + \mathbf{w} \tag{3}$$

- **in the continuum theory of continuously distributed dislocations** the role of displacement gradient $\nabla \mathbf{u}$ is taken by a continuous field of dislocation density tensor determined as

$$\alpha \overset{df}{=} -\operatorname{curl} \beta \tag{4}$$

where in the index notation the differential operator *curl* reads $\alpha_{ij} = \beta_{ik,l}\, e_{jkl}$, the comma means here the so-called covariant differentiation, and e_{jkl} is the alternating tensor (permutation symbol).

In both approaches, similar to Eq. (2), the total distortion field

$$\beta_{tot} = \beta + \beta_{pl} \tag{5}$$

has to satisfy the following compatibility condition

$$\operatorname{curl} \beta_{tot} = 0 \tag{6}$$

By substitution of (4) and (5) into (6) it can be shown that

$$\operatorname{curl} \alpha + \operatorname{curl} \alpha_{pl} = \operatorname{curl} \beta_{tot} = \operatorname{curl} (\nabla \mathbf{u}) = 0 \tag{7}$$

or simply $\operatorname{curl} \beta = -\operatorname{curl} \beta_{pl}$, cf. (6) and (1). Thus, the dislocation density tensors α can be defined alternatively to (4) as

$$\alpha = \operatorname{curl} \beta_{pl} \tag{8}$$

It is worth mentioning here that in the dislocation theory, another tensorial measure of strain (and/or rotation) incompatibilities are applied

$$\eta \overset{df}{=} \operatorname{inc} \beta = -\operatorname{inc} \beta_{pl} \tag{9}$$

where η means incompatibility tensor related to the permanent rearrangement of the crystal structure related to discontinuity in the displacement field. In the index notation the differential operator inc reads

$$\eta_{ij} = \beta_{kl,mn}\, e_{kmi}\, e_{lnj} \tag{10}$$

Unfortunately, large elastic deformation of the crystal lattice in the close vicinity of the defect makes classical elastic model based on Hooke's law and linear strain measure no longer very accurate. Except that, deformation decomposition into elastic and plastic parts justifies the existence of an intermediate configuration also called the local lattice configuration of the body $\hat{\mathbf{x}}$, see [26]. Thereupon only the use of a mathematical model which takes into account finite deformation allows a description of the crystal with defects in a proper way. Thereby, instead of displacement gradient we may use deformation gradient $\mathbf{F}_{tot}$ decomposed multiplicatively into lattice (elastic) deformation $\mathbf{F}$ and plastic deformation $\mathbf{F}_{pl}$.

$$\mathbf{F}_{tot} = \mathbf{F}\,\mathbf{F}_{pl} \tag{11}$$

Lattice deformation $\mathbf{F}$ denotes here a thermodynamically reversible deformation of the crystal structure or heterostructure caused by a lattice mismatch and related elastic relaxation. In the chemically homogeneous structures lattice deformation is identified with the elastic one. In most cases it is assumed that chemical deformation tensor in the main crystallographic orientation has only on-diagonal components. If the distortion is the spatial gradient of the displacement vector

$$\beta = \frac{\partial \mathbf{u}}{\partial \mathbf{x}} = \mathbf{I} - \mathbf{F}^{-1}, \quad \hat{\beta} = \frac{\partial \mathbf{u}}{\partial \hat{\mathbf{x}}} = \mathbf{F} - \mathbf{I} \tag{12}$$

we may write that plastic (initial) distortions are equal

$$\hat{\beta}_{pl} = \mathbf{F}_{pl} - \mathbf{I} \tag{13}$$

By integrating over the closed contour in a proper configuration (initial or actual) we can obtain spatial or true Burgers vectors, $\mathbf{b}$ or $\hat{\mathbf{b}}$, respectively. We may write then

$$\mathbf{b} = \oint_c d\mathbf{x} = \int_O \mathbf{F}\, d\hat{\mathbf{X}} = \int_O \left(1 + \hat{\beta}\right) d\hat{\mathbf{X}} \tag{14}$$

$$-\hat{\mathbf{b}} = \oint_C d\mathbf{X} = \int_O \mathbf{F}^{-1}\, d\hat{\mathbf{x}} = \int \left(1 + \beta\right) d\hat{\mathbf{x}} \tag{15}$$

where *o* i *O* denote, respectively, open contours in an actual and initial configuration, while *c* i *C* mean closed loops over the analogous configuration. Strict and mutually reversible formula for distortions measured in different configurations is as follows

$$\hat{\beta} = \left(\mathbf{I} - \beta\right)^{-1} - \mathbf{I} \tag{16}$$

5.3. Continuous and Atomistic Reconstruction of Dislocations

The displacement field around dislocation and its mathematical description has been a very popular problem of the continuum theory of dislocations for many years. The first complete solution for the displacement field was given by Love in 1927 [21] and later on it was modified by several authors, see [22, 23, 4]. The basic assumption of the solution is that the crystal is an isotropic elastic continuum and the edge and screw components of the Burgers vector coincide, respectively, with X and Z axes of the local coordinate system, and the dislocation line is coaxial with Z. In such a case we may use following formulae for the displacement field

$$\begin{aligned} u_x &= \frac{\hat{b}_x}{2\pi}\left(\arctan\frac{y}{x} + \frac{xy}{2(1-\nu)(x^2+y^2)}\right) - \frac{\hat{b}_x}{2} \\ u_y &= \frac{\hat{b}_x}{2\pi}\left(\frac{1-2\nu}{4(1-\nu)}\ln\left(x^2+y^2\right) + \frac{x^2-y^2}{4(1-\nu)(x^2+y^2)}\right) \\ u_y &= \frac{\hat{b}_z}{2\pi}\arctan\frac{y}{x} - \frac{\hat{b}_x}{2} \end{aligned} \tag{17}$$

where $\hat{b}_x$, $\hat{b}_z$, and ν mean the edge and screw components of the true Burgers vector, and Poisson ratio. x, y coordinates denote the position of the dislocation line perpendicular to the xy-plane. On the half-plane defined by coordinates equal ($x < 0$, $y = 0$) there is a discontinuity in the displacement field, corresponding to the Burgers vector b of the dislocation. In Fig. 1 there are shown different atomic configurations of the the aluminium nitride crystal — a common semiconductor with hexagonal symmetry. The

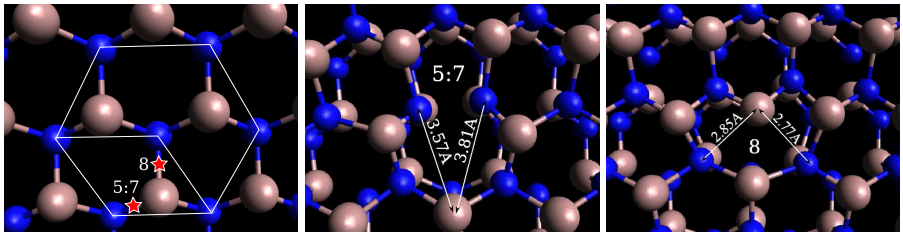

Fig. 1. Atomic configuration in hexagonal crystal AlN along [0001] axis: a) ideal crystal, b) edge dislocation core for 5 : 7-ticked point, b) edge dislocation core for 8-ticked point

first configuration corresponds to the perfect crystal and the next two configurations present different types of edge dislocation. Burgers vector of the edge dislocation is equal to the lattice parameter $a = 3.112$Å in main crystallographic orientation $\langle 11\bar{2}0 \rangle$. These two dislocation cores differ in the position of the dislocation line, which corresponds to the singularity in Love's solution. As we can see, the difference in

the position taken by the same dislocation line makes a significant change in its core structure, while the continuous displacement field is the same, see Eqs. (17). Also, noticeable asymmetry of the atomic position in the sub-figures Fig. 1b and Fig. 1c is visible, see inter-atomic distances marked in the figures.

Another way to determine the source distortion field around dislocation is computer analysis of the HRTEM images, see for example [18, 32]. In that case we have to deal with single spots in the diffraction pattern of the structure visible in the HRTEM image (the reciprocal space). Small enough aperture around single diffraction pick related to the strict crystallographic orientations allows us to extract the displacement field and phase along that orientation. Next, by applying Geometric Phase Method (GPM), we can calculate a discreet distribution of the source distortion field. The resolution of the resultant map of source distortions depends on the resolution of source HRTEM image and may reach a small fraction of Å - even two orders of magnitude less than a crystal lattice parameter. The experimentally measured displacement field around the edge dislocation, measured by HRTEM [18], has a significant asymmetry between the upper and lower parts of the displacement. Such asymmetry in the experimentally measured elastic deformation of the crystal can be explained by a nonlinear behaviour of the crystal structure, which is harder for compressive loadings and weaker for elongation. The same behaviour for atomic interactions is predicted by atomic potentials and is visible in the bonding force chart. The bonding force is the derivative of the bonding energy, so such behaviour is the effect of the form of bonding energy function, see Fig. 2.

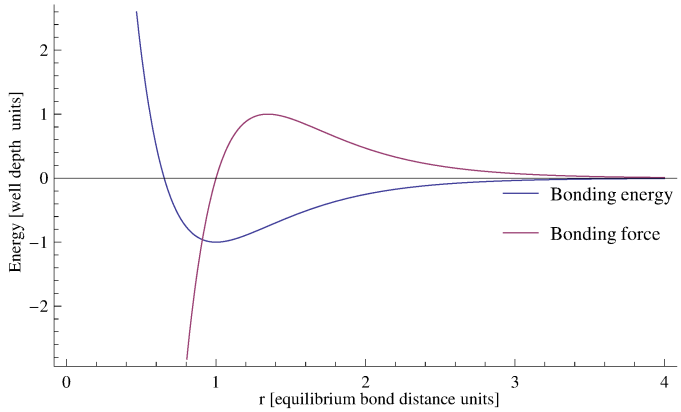

Fig. 2. Bonding energy and bonding force calculated for the Morse atomic potential, see [27]

Unfortunately, the theoretical displacement field around the edge dislocation (u_z = 0, see Eqn. (17)) based on Love's solution, rewritten to the cylindrical coordinate system has the form

$$u_x = \frac{b_x}{2\pi}\left(\theta + \frac{\sin 2\theta}{4(1-\nu)} - \pi\right) \tag{18}$$

$$u_y = -\frac{b_x}{2\pi}\left(\frac{1-2\nu}{4(1-\nu)}\ln r^2 + \frac{\cos 2\theta}{4(1-\nu)}\right) \tag{19}$$

and is fully symmetric, see comparison of the experimental and theoretical displacement fields in [18, 19].

Because crystal nonlinearity seems to be a very important factor in the case of crystal modelling, we have to take it into account. To do that, we may apply a mathematical model which deals with geometric (kinematic relation) and physical (constitutive equation) nonlinearity. The most popular nonlinear kinematic relation was proposed by Seth [28] and further by Hill [29] and it is known as a generalized strain measure

$$\hat{\varepsilon} = \begin{cases} \frac{1}{m}\left(\mathbf{U}^m - \mathbf{I}\right) & m \neq 0 \\ \ln\left(\mathbf{U}\right) & m = 0 \end{cases} \tag{20}$$

where, $\mathbf{U}$ is the right stretch tensor obtained from the polar decomposition of elastic deformation tensor $\mathbf{F} = \mathbf{R}\,\mathbf{U}$. Exponent m defines the strain measure and usually is an integer number.

To take into account the physical nonlinearity of the crystal let's use the following constitutive equation for stress

$$\hat{\sigma} = \hat{\mathbf{c}} : \hat{\varepsilon} + \frac{1}{2}\hat{\varepsilon} : \hat{\mathbf{C}} : \hat{\varepsilon} + \ldots \tag{21}$$

where $\hat{\mathbf{c}}$, $\hat{\mathbf{C}}$ mean stiffness tensors of the second and third order elasticity. We may now write the complete formula for the Cauchy stress $\boldsymbol{\sigma}$,

$$\sigma = \mathbf{R}\left(\hat{A} : \underbrace{\left(\hat{\mathbf{c}} : \hat{\varepsilon} + \frac{1}{2}\hat{\varepsilon} : \hat{\mathbf{C}} : \hat{\varepsilon} + \ldots\right)}_{\hat{\sigma}}\right)\mathbf{R}^T \det \mathbf{F}^{-1} \tag{22}$$

where $\hat{A}$ is some geometric function of strain, $\hat{A} = \hat{A}(\hat{\varepsilon})$, taking a role of transformation tensor for stresses in different lattice configurations, see [30]. Taking into account the above constitutive relations we can write that the Cauchy stress is a nonlinear function of the displacement field, its gradient, and source distortions as follows

$$\sigma = \sigma\left(\mathbf{u}, \nabla\mathbf{u}, \hat{\beta}_{pl}\right) \tag{23}$$

A boundary-value problem for an elastic crystal with dislocations, discrete and/ or continuously distributed, can be stated in the form of coupled displacement and distortion fields. Contrary to the displacement-type degrees of freedom these distortion-type degrees corresponding to the input source distortions are fixed. So, our FE method algorithm has the following matrix form, see [31]

$$[\mathbf{P}][\mathbf{a}]=[\mathbf{f}],\quad \mathbf{P}=\left[\int_{\mathbf{0}}^{v}\nabla^{T}\mathbf{W}\sigma dv\right],\quad \mathbf{a}=\begin{bmatrix}\mathbf{u}\\ \hat{\beta}\end{bmatrix},\quad \mathbf{f}=\left[\int_{\mathbf{0}}^{\partial_v}\mathbf{W}\sigma ds\right] \tag{24}$$

P means stiffness matrix, **a** - degrees of freedom vector, **f** - nodal loadings vector, and **W** - weighting function. As stated above, see Eq. (23), Cauchy stress **σ** is the nonlinear function of the displacement field **u**, its gradient $\nabla\mathbf{u}$, and source distortions $\hat{\beta}$.

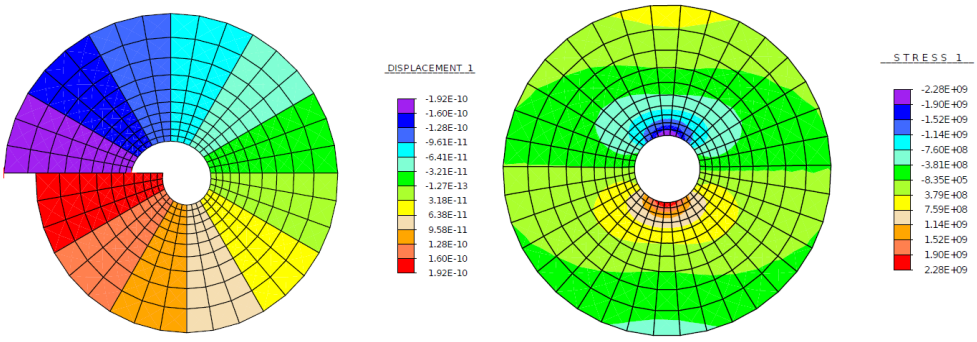

Fig. 3. Circular plate with a hole: a) displacement field, b) residual stresses

The idea and the application of source distortions can be illustrated by the problem of a circular plate with a hole, as sketched in Fig. 3. The hole in the centre of the plate is to avoid the singularity appearing in Eqs. (17). The natural state (stress free) of the plate with acut is presented in Fig. 3a. The colour map in this figure corresponds to the horizontal displacement field necessary to deform the initial plate to get the fully circular shape of the plate as shown in Fig. 3b. The iInitial plate with a cut after deformation became smooth and fully circular but residual stresses appear, see Fig. 3b. Such plate is just an analogue to Volterra's edge dislocation, where the displacement of the plate edge u_x corresponds to the Burgers vector of dislocation **b**.

A similar deformation of the plate can be obtained by inelastic (plastic) deformation using source distortions, which allows us to avoid residual stresses and get stress free permanent deformation of the plate. Source distortions as derivatives of Eqs. (17) have the following form

$$\beta_{xx}=\frac{-\hat{b}_x}{2\pi}\frac{(3-2\nu)x^2y+(1-2\nu)y^3}{2(1-\nu)\left(x^2+y^2\right)^2} \qquad \beta_{xy}=\frac{\hat{b}_x}{2\pi}\frac{(3-2\nu)x^3+(1-2\nu)xy^2}{2(1-\nu)\left(x^2+y^2\right)^2}$$

$$\beta_{yx}=\frac{-\hat{b}_x}{2\pi}\frac{(1-2\nu)x^3+(3-2\nu)xy^2}{2(1-\nu)\left(x^2+y^2\right)^2} \qquad \beta_{yy}=\frac{\hat{b}_x}{2\pi}\frac{(1+2\nu)x^2y-(1-2\nu)y^3}{2(1-\nu)\left(x^2+y^2\right)^2} \quad (25)$$

$$\beta_{zx}=\frac{-\hat{b}_z}{2\pi}\frac{y}{x^2+y^2} \qquad \beta_{zy}=\frac{\hat{b}_z}{2\pi}\frac{x}{x^2+y^2}$$

Using this methodology we are able to reconstruct any type of dislocation in the crystal structure, e.g. in the silicon carbide 2H-SiC. The reconstructed atomic structure for the edge and screw dislocations are presented in Fig. 4.

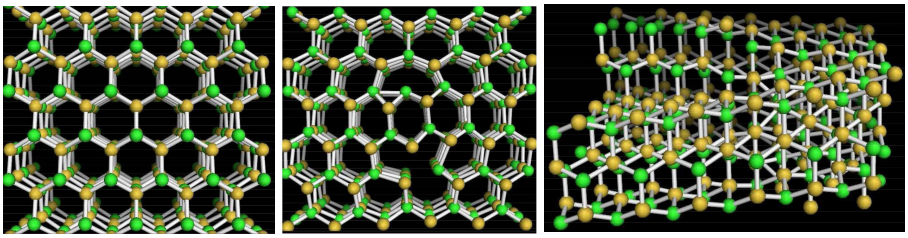

Fig. 4. Ball and stick model of 2H-SiC crystal with defects: a) initial (ideal) crystal structure, b) edge dislocation, c) screw dislocation (side view)

In the case of analytical modelling of dislocations in the crystal using Eqs. (17), (25) we have to assume its crystallographic orientation and proper dislocation core radius. As mentioned above, the analytical equations allow modelling dislocation whose components of Burgers vector coincide with *X* and *Z*-axes of the local coordinate system. Therefore, to model any chosen dislocation it is necessary to transform the coordinate system to get its coincidence with Burgers vector (and simultaneously reset by component of Burgers vector). Then, *Z*-axis straight-line dislocation can be described by a dislocation density function as

$$\alpha=\alpha(r)=\begin{bmatrix}0 & 0 & \alpha_x\\ 0 & 0 & 0\\ 0 & 0 & \alpha_z\end{bmatrix},\ \text{where } \mathbf{b}=[b_x,\,0,\,b_z],\quad r=\sqrt{x^2+y^2} \qquad (26)$$

The dislocation core radius is a very important parameter of the analytical modelling of dislocation. Within the core radius of the dislocation line the limit of the applicability of classical Love's equations is assumed. Inside the core another set of equations, e.g. based on polynomial expansion, should be used, i.e. [25]. The proposed equations, except obvious compatibility with classical Love's equation, should also satisfy the following compatibility condition for the displacement field on the dislocation core surface

$$\beta^c = \nabla \mathbf{u}\,, \quad \text{grad}\,\beta^c = \nabla^2 \mathbf{u}\,, \quad \text{inc}\,\beta^c = 0 \tag{27}$$

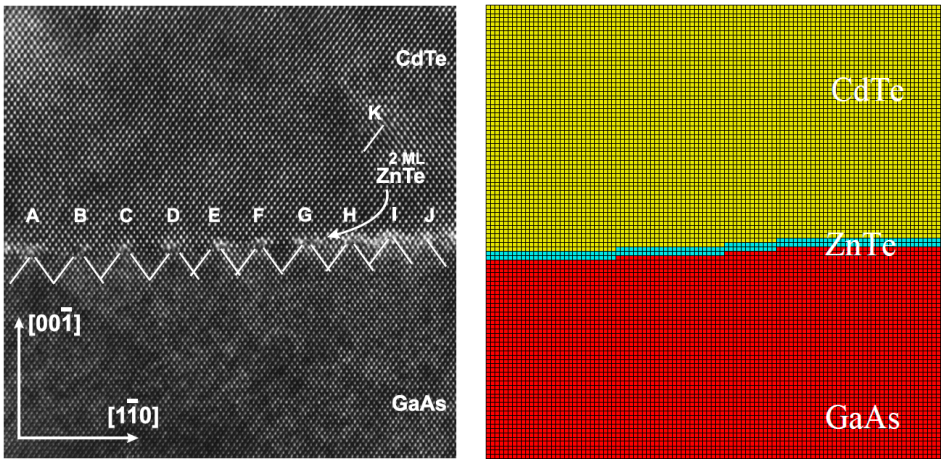

Fig. 5. GaAs/CdTe heterostructure with ZnTe wetting layer: a) HRTEM image with locations of dislocations highlighted by dashes showing missing crystalline half-planes, b) assumed FE mesh with material distribution marked by a colour map, see [31]

5.4. Reconstruction of Dislocation Networks

In real structures, dislocations very often create specific spatial networks or complexes, e.g. low-angle grain bound- aries, misfit dislocations, etc. Misfit dislocations are typical of the mismatched heterostructure and they are present on the interface between layers. In the case of GaAs/ZnTe/CdTe heterostructure, presented in Fig. 5, the mismatch between the layer and substrate is about 14.6%, which is rather a high value. Therefore, an extra wetting layer (ZnTe crystal) with an average lattice parameter is used to reduce the problem of layer delamination. Such interface contains high density of crystal defects, which makes an analytical approach very toilsome, especially if the orientation of Burgers vectors differs from each other (the need of coordinate system transformation every time). So, instead of the analytical approach, an extraction of the source distortions directly form HRTEM images using the computer analysis is applied. The calculated displacement fields in the crystal structure for selected crystallographic orientations are shown in Fig. 6. The lower part of the structure (the substrate - GaAs) was used as a reference, and extra atomic half-planes of the CdTe layer (smaller lattice parameter) are clearly visible in the displacement field of the upper part. The source distortions were extracted from the TEM image by differentiation of these displacement fields, see Fig. 6.

If we zoom in the dislocation cores present on the GaAs/CdTe interface (Fig. 5) it is possible to measure Burgers vectors of these dislocations and determine the dislocation

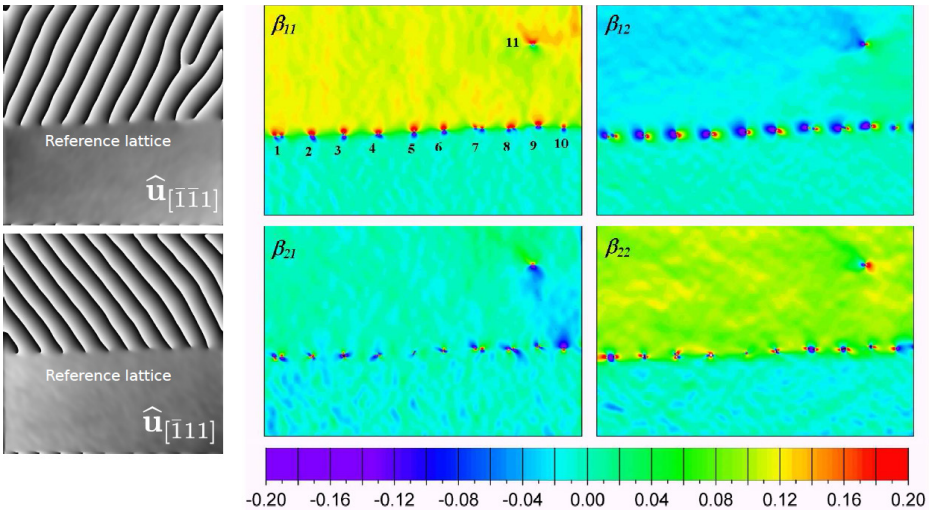

Fig. 6. Components of the displacement and distortion fields extracted form the experimental HRTEM images [32]

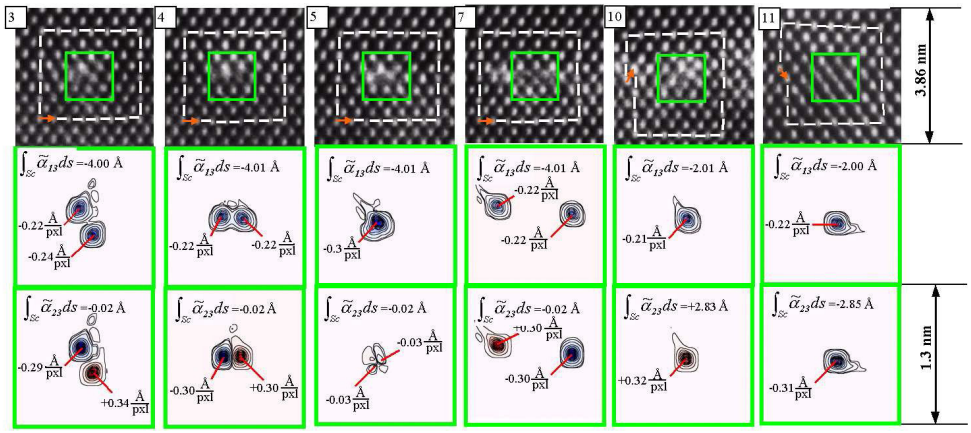

Fig. 7. Analysis of the dislocation cores present on the GaAs/CdTe heterostructure interface

density distribution. In Fig. 7 a zoomed vicinity of a few dislocations on the interface is shown. The numbering of dislocations corresponds to the numbering in Fig. 5 [32]. The green frame indicates the dislocation core, while the white frame denotes Burgers contour with complementary orange Burgers vector. The lower panel shows the dislocation density analysis which allows determining the type of dislocation. Burgers vector, marked as an orange arrow, is determined according to the left-hand finish-start (LHFS) convention.

Most dislocations on the interface are of the edge type (Burgers vector is $\frac{1}{2}\left[1\,\bar{1}0\right]$ and

lies in the figure plane - perpendicularly to the electron beam direction). Dislocations *J* and *K* are of mixed type and their Burgers vector ($\frac{1}{2}[10\bar{1}]$ or $\frac{1}{2}[0\bar{1}1]$) makes a 60° angle with the dislocation line parallel to the electron beam. However, detailed analysis of edge dislocations (see Fig. 7) reveals that each edge dislocation is composed of two 60°-type mixed dislocations with a consistent edge and opposite screw components. It is evident for **C**, **D**, and **G** ddislocations and hardly visible for **E** dislocation. Such dislocations are called a Lomer dislocation and in our case we may write the following dissociation formula

$$\frac{1}{2}[1\bar{1}0]=\frac{1}{2}[10\bar{1}]+\frac{1}{2}[0\bar{1}1] \quad \text{or} \quad \frac{1}{2}[101]+\frac{1}{2}[0\bar{1}\bar{1}] \tag{28}$$

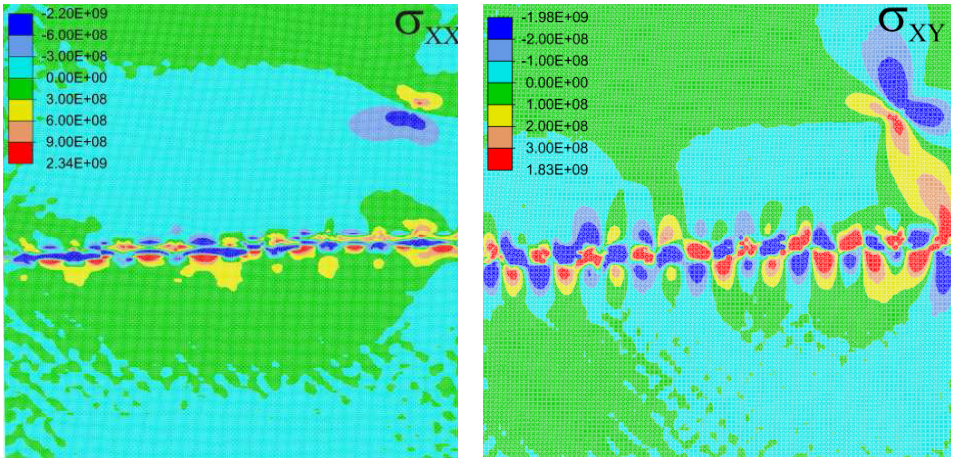

Fig. 8. Residual stresses calculated on the basis of computer analysis of HRTEM images, see [32]

In the case of computer analysis of HRTEM images we are able to determine only a 2D information on dislocations, while they are real 3D objects. The data concerning the direction perpendicular to TEM image were lost already at TEM image creation stage. Therefore, we have to find another way to complete the obtained distortion field, and get a full 3D description of the dislocation. To do that we may assume that the ratio between components of the distortion field is the same as the ratio between components of Burgers vector (in our case thelost screw and visible edge components). Let's write decomposition of Lomer dislocation composed by a pair of two 60° dislocations in the local coordinate frame related to HRTEM image, see crystallographic orientation in Fig. 5

$$\begin{aligned} &\frac{1}{2}[10\bar{1}]=\frac{1}{4}[1\bar{1}0]+\frac{1}{2}[00\bar{1}]+\frac{1}{4}[110] \\ \text{and} \quad &\frac{1}{2}[0\bar{1}1]=\frac{1}{4}[1\bar{1}0]-\frac{1}{2}[00\bar{1}]-\frac{1}{4}[110] \end{aligned} \tag{29}$$

The ratio between the lengths of Burgers vector components gives the following relation

$$\hat{b}_{[110]} = \frac{\sqrt{2}}{2}\hat{b}_{[00\bar{1}]} \tag{30}$$

So, for the image extracted from TEM the in-plane components of the distortion field β_{xx}, β_{xy}, β_{yx}, β_{yy} (ssee, Fig. 6), and the assumed relation for the revealed Lomer dislocations we may write the following formula for the complete tensor o source distortions

$$\hat{\beta} = \begin{bmatrix} \hat{\beta}_{xx} & \hat{\beta}_{xy} & 0 \\ \hat{\beta}_{yx} & \hat{\beta}_{yy} & 0 \\ \frac{\sqrt{2}}{2}\hat{\beta}_{yx} & \frac{\sqrt{2}}{2}\hat{\beta}_{yy} & 0 \end{bmatrix} \tag{31}$$

Such relation results also in a similar relation for the dislocation density components $\hat{\alpha}_{[110]} = \sqrt{2}/2\,\hat{\alpha}_{[00\bar{1}]}$. Let's apply such distortion field to the boundary value problem of the misfit dislocations network at the *GaAs*/*ZnTe*/*CdTe* heterostructure interface. By solving the boundary-value problem we get residual stresses in the heterostructure and the spatial distribution is presented in Fig. 8.

5.5. Finite Deformations

The analytical approach to the dislocation reconstruction described in Section 3 is based on the linear elasticity theory and has a limited application and accuracy in the dislocation core. There is no doubt it is fast, simple and quite accurate but their limits follow the initial assumption (push forward transformation) and used material description (linear theory of elasticity). To improve this solution we have to use pull back transformation and take into account the finite deformation of the crystal structure definitely arising around the core. The problem with pull back transformation concerns the unknown configuration from which we have to go back to the ideal crystal. Therefore, instead of the existing formulae [21, 22]

$$\mathbf{u}(\mathbf{x}) = \mathbf{f}(\mathbf{x}) \tag{32}$$

we should use the following relation

$$\mathbf{u}(\mathbf{X}) = \mathbf{f}\,(\mathbf{x}(\mathbf{X})) = \mathbf{f}(\mathbf{X} + \mathbf{u}(\mathbf{X})) \tag{33}$$

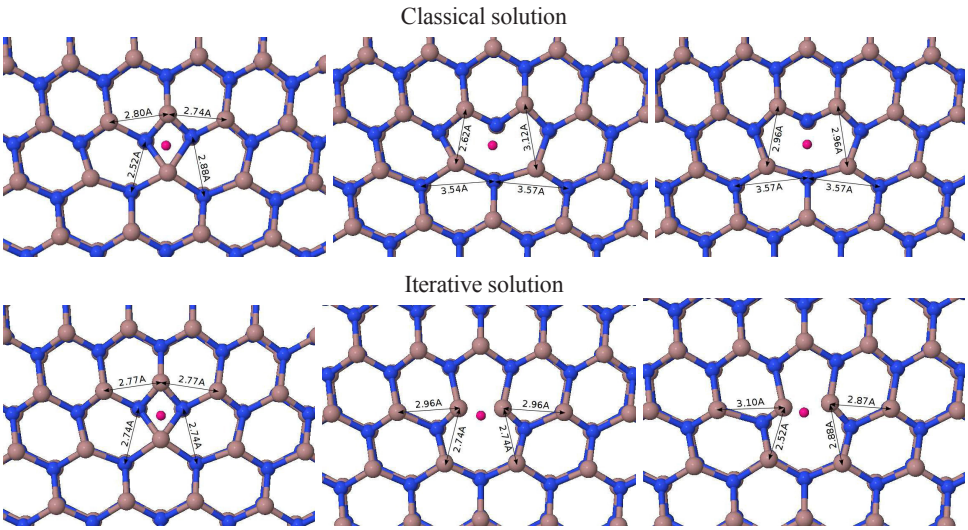

Fig. 9. Dislocation configurations of deformed GaN crystal in the case of edge dislocation. Upper panel shows classical solution, lower panel presents iterative solution. Insertion point for dislocations is marked as a red dot. Additionally, inter-atomic distances are shown for informative purposes

The nonlinear equation above can be solved using an iterative method

$$\mathbf{u}^{i+1} = \mathbf{u}^{i} + \Delta\mathbf{u}^{i+1} \tag{34}$$

In the case of Newton-Raphson method the $(i + 1)$-step adjustment of the displacement $\Delta\mathbf{u}$ is

$$\Delta\mathbf{u}^{i+1} = -\left(\frac{\partial\Psi(\mathbf{X},\mathbf{u})}{\partial\mathbf{u}}\right)^{-1}_{\mathbf{u}=\mathbf{u}^{i}} \Psi\left(\mathbf{u}^{i}\right) \tag{35}$$

where correction factor Ψ is

$$\Psi(\mathbf{X},\mathbf{u}) = \mathbf{u} - \mathbf{f}(\mathbf{X} + \mathbf{u}) \tag{36}$$

If we assume that locally β equals $\nabla\mathbf{u}$ we obtain

$$\frac{\partial\Psi(\mathbf{X},\mathbf{u})}{\partial\mathbf{u}} = = 1 - \beta(\mathrm{x}) \tag{37}$$

Finally, we may write an iterative formula for the displacement which describes the jump from the initial configuration (as a classical solution) and take into account the change of the actual configuration

$$\Delta\mathbf{u}^{i+1}(\mathbf{X}) = -\left[1-\beta\left(\mathbf{X}+\mathbf{u}^{i}\right)\right]^{-1}\left[\mathbf{u}^{i} - \mathbf{f}\left(\mathbf{X}+\mathbf{u}^{i}\right)\right] \tag{38}$$

By taking into account the configuration change, it is possible to reduce the asymmetry arising in the displacement field, see Fig. 1b,c. Due to the specific nature of the equations used in our iterative methodology, see Eqs. (17), an improvement is observed only for the edge and mixed type of the dislocation. Screw dislocation configuration can not be attuned the iterative methodology presented above due to the fact that displacement components u_x, u_y do not depend on x_z position nor does b_z component of Burgers vector affect u_x, u_y displacements. The improved dislocation configurations obtained using the iterative procedure are shown and compared with the classical solution in Fig. 9.

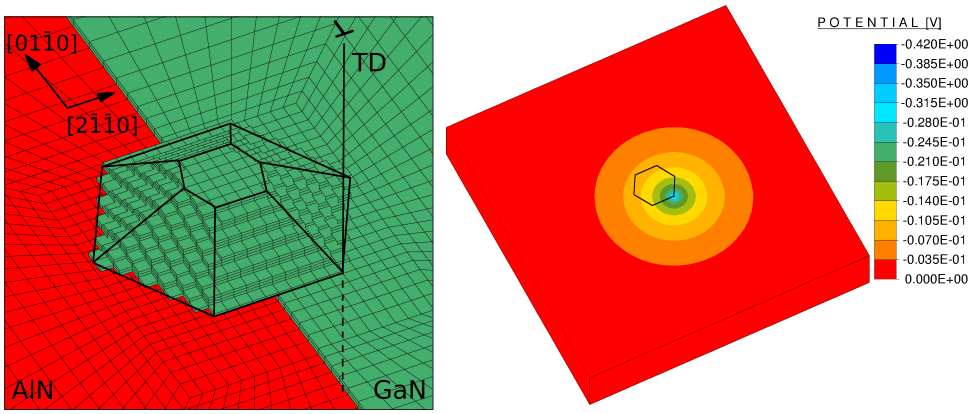

Fig. 10. Left: Zoom in on the finite element grid used to model polar QD nucleated near TD of edge type. Upper part of AlN matrix has been removed for simplicity. Also, crystallographic orientations and location of dislocation line are indicated. Right: electrostatic potential distribution around edge type of TD. In both cases, wire-frame corresponds to QD edges

5.6. GaN Quantum Dot Nucleated near Threading Dislocation

Wurtzite III-nitrides (binary, ternary and quaternary compounds of GaN/AlN/InN) are considered as promising optically active structures for the application in the future optoelectronic devices due to their large and tunable band gap, and high tolerance to work in a harsh environment [33]. Wurtzite type of crystals, apart from other commonly used semiconductors, has a unique spontaneous polarisation related to the growth direction. This feature, together with piezoelectric polarisation, induces a strong built-in electric field in these structures. The built-in electric field has been shown to strongly affect the optoelectronic properties of light emitting devices [34, 35]. Initially, to develop the first blue light emitting devices multiple InGaN/GaN quantum wells were used [8]. Unfortunately, the lack of suitable substrates and high lattice mismatch introduce defects into the heterostructure in

the form of TD. The typical density of TDs in III-nitrides is in the range of 10^9–10^{11} cm^{-2} [33, 36] and through advanced growth techniques can be decreased to 10^7 cm^{-2}. Because TD affects the quantum efficiency of light emitting devices based on QWs and can be detrimental for their lifetime, several approaches have been developed to mitigate this problem, e.g. improvements in the growth process and advanced dislocation reducing techniques as, for example, epitaxial lateral overgrowth. Quite a different approach to improve the quality of optically active structures is to use QD as radiative recombination centres, e.g. self-assembled GaN/AlN QDs grown in polar, nonpolar or semipolar directions [36, 37, 38]. The zero–dimensional nature of QDs permits three–dimensional particle–hole localization and from that the design of interesting (and useful) optoelectronic devices, i.e. light emitters/detectors. The explicit correlation between dislocation arrangement and QD formation [36] suggests that TD in such heterostructures may facilitate seed processing and growth of QD. Unfortunately, their presence still promote non-radiative recombination centres which reduce the optical output, heat-up the device, and reduce the operational lifetime.

Progress in experimental techniques based on electron holography enables the measurement of the electrostatic potential in a defective heterostructure, e.g. potential related to free charges trapped by dangling bonds in a dislocation core. The potential distribution reported for the edge–type dislocation in GaN crystals has the peak value in the range of $-0.2 \div -3.0$V with the axisymmetric range of about $15 \div 50$ nm [39, 40]. The corresponding electron density of the dislocation line is between $0.3 \div 2.0$ electrons per GaN lattice parameter.

In this discussion we consider a Wurtzite heterostructure, consisting of the polar GaN quantum dot in the AlN matrix, as if it was a three–dimensional coherent inclusion. The QD morphology can be reliably obtained from TEM observations, see [36]. Fig. 10a gives an illustration of the hexagon-based truncated pyramid geometry of the polar QD nucleated near perfect edge type TD with Burgers vector $\mathbf{b} = 1/3\left[\bar{2}110\right]$. Local source distortions around the TD line localized at the corner of the bottom facet of QD were modelled using the analytical approach, see Eqs. (25). The size of QD is 17×4.1 nm respectively for bottom and top facets while the height is 3.6 nm. A cuboidal AlN matrix is assumed to be ~10 times larger, so the GaN/AlN volume ratio is about 10^{-3}. That allows us to assume that our heterostructure is mechanically and electrically isolated. In the specific case, mutual diffusion between GaN and AlN is limited, so the edges are satisfyingly clear and sharp. The finite element grid is constructed of non–affine hexahedral elements whose geometry are locally attuned to accommodate the real–space geometry of the buried QD and material identification is assigned to each element. The dislocation charge density was assumed to be $0.3e/c$ which corresponds to the potential peak value -0.42V. The radius of the axisymmetric extent of the potential, following [40], was truncated to 35 nm, see Fig. 10b.

To calculate the coupled elastic-electric problem the following coupled equilibrium equation set must be solved: div [**σ**] = [**0**] and div [**D**] = 0. Cauchy stress **σ** and electric displacement **D** satisfy the following constitutive relations

$$\sigma_{ij} = C_{ijkl}\varepsilon^{e}_{kl} - e_{kij}E_k \tag{39}$$

$$K_k = e_{kij}\varepsilon^{e}_{ij} + e_{ki}E_i + P^{sp}_k \tag{40}$$

The elastic strain $\boldsymbol{\varepsilon}^{e}$ is related to lattice strain and chemical strain by $\boldsymbol{\varepsilon}^{e} = \boldsymbol{\varepsilon} - \boldsymbol{\varepsilon}^{ch}$, while the electric field is $\mathbf{E} = -\text{grad}\,\phi$. The lattice strain is calculated from the lattice deformation tensor after the decomposition of the deformation gradient, see Eq. (11). Tensors of physical moduli **C**, **e**, *e*, and supplement spontaneous polarisation $\mathbf{P}^{sp}$ define the elastic and electric properties of crystals [41]. The fully coupled piezoelectric pair of constitutive equations is solved for the boundary conditions in which the loading forces and charges on surfaces vanish for the vector *n* normal to the AlN matrix surfaces. The system of equations is solved using a direct solver based on a sparse Gauss elimination algorithm in FEAP program [42].

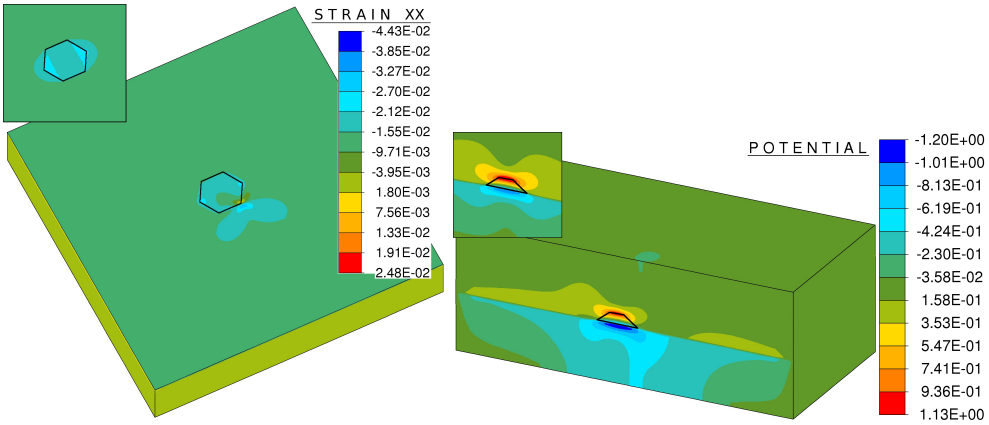

Fig. 11. Elastic strain ε_{xx} ([0001] cross-section) and electrostatic potential ([$2\bar{1}\bar{1}0$] cross-section) distribution around polar QD nucleated near the TD of the edge type. dditional small windows show the strain and electrostatic potential maps for stand-alone QD. The wire-frame corresponds to QD edges

The resultant strain field and potential is presented in Fig. 11. QD is strained in (0001)–plane and slightly elongated along the [0001]–axis. The compression in the QD area is an effect of the elastic relaxation driven by lattice mismatch between QD and matrix crystals. The compression peak values correspond to lattice mismatch values, which in given crystallographic orientation are (−2.47%,−2.47%,−4.07%). The spatial distribution of the strain components are locally affected by the lattice distortion around the dislocation line. Because of the differences between AlN lattice

and GaN inclusion, QD preferentially nucleate in the vicinity of TD, where AlN matrix is locally attuned to GaN crystal. This promotes QD growth and slightly reduce its energy. The presence of the charged dislocation near QD and potential interaction causes a nonlinear shift of the built-in electrostatic potential along z-direction. The negative shift of the electrostatic potential causes a small shift in the band energies. Calculations show a small decrease in the effective band-to-band transition energy calculated in the centre of QD, see Ref. [43]. Together, with carrier localisation it may have a measurable effect on the optical spectrum of such QDs.

5.7. Summary

The procedures for reconstruction of discrete crystal structure affected by a set of dislocations as well as the modelling of coupled fields effect in semiconducting heterostructures presented here set an example of a deterministic method based on the nonlinear field theory of dislocations and elasticity or piezoelectricity. The problem of dislocation modelling is located on the border of continuum mechanics and discrete (atomistic) modelling of crystal lattice periodicity. In computer modelling (molecular statics/dynamics, finite element analysis) the crucial problem is to create an accurate spatial structure of the crystal with incorporated defects. There are two complementary approaches: theoretical and experimental. The choice depends on the problem considered and of course on the availability of high accuracy data, e.g. experimental measurements by TEM techniques.

The methodology presented above can be used to create a new advanced and comfortable tool or just extend existing pre-processors, e.g. PATRAN, GiD in order to create an accurate initial atomic configuration used in modelling of the crystal structure (Abaqus, FEAP, LAMMPS). The iterative solver has been programmed in Visual Editor of Crystal Defects (VECDs, see [44]) and can be used as a pre-processor or viewer during atomistic modelling.

Acknowledgment

This research was supported by the projects N N519 647640 founded by the Polish Ministry of Science and Higher Education.

References

[1] Taylor G.I., The Mechanism of Plastic Deformation of Crystals. Part I. Theoretical, Proc. R. Soc. A 145 (1934), 362.
[2] Orowan E., Zur Kristallplastizität, Z. Phys. 89 (1934), pp. 605-659.
[3] Polanyi M., Über eine Art von Gitterstörung, die einem Kristal plastisch machen könnte, Z. Phys. 89 (1934), pp. 660-664.
[4] Hirth J.P. and Lothe J., Theory of Dislocations, Wiley, New York, 1982.
[5] Shockley W., Dislocations and edge states in the diamond crystal structure, Phys. Rev. 91 (1953), 228.
[6] Read W.T., Theory of dislocations in germanium, Phil. Mag. 45 (1954), pp. 775-796.
[7] Dingle R., Shaklee K.L., Leheny R.F. and Zetterstrom R.B., Stimulated Emission and Laser Action in Gallium Nitride, Appl. Phys. Lett. 19 (1971), pp. 5-7.
[8] Nakamura S., Senoh M., Nagahama S., Iwasa N., Yamada T., Matsushita T., Kiyoku H. and Sugimoto Y., InGaN-Based Multi-Quantum-Well-Structure Laser Diodes, Jpn. J. Appl. Phys. 35 (1996), pp. L74-L76.
[9] Wright A.F. and Grossner U., The effect of doping and growth stoichiometry on the core structure of a threading edge dislocation in GaN, Appl. Phys. Lett. 73 (1998), pp. 2751–2754.
[10] Abell J. and Moustakas T.D., The role of dislocations as nonradiative recombination centers in InGaN quantum wells, Appl. Phys. Lett. 92 (2008), 091901.
[11] Béré A., Chen J., Ruterana P., Serra A. and Nouet G., The atomic configurations of the ~a threading dislocation in GaN, Comp. Mater. Sci. 24 (2002), pp. 144-147.
[12] BlumenauA.T., Fall C.J., Jones R., Oberg S. Frauenheim T. and Briddon P.R., Structure and motion of basal dislocations in silicon carbide, Phys. Rev. B 68 (2003), pp. 174108-1–174108-14.
[13] Belabbas I., Chen J. and Nouet G., A new atomistic model for the threading screw dislocation core in wurtzite GaN, Comp. Mater. Sci. 51 (2011), pp. 206-216.
[14] Figielski T., Dislocations as electrically active centres in semiconductors - half a century from the discovery, J. Phys.: Condens. Matter 14 (2002), pp. 12665–12672.
[15] Liu J.Q., Skowroński M., Hallin C., Söderholm R. and Lendenmann H., Structure of recombinationinduced stacking faults in high-voltage SiC p-n junctions, Appl. Phys. Lett. 80 (2002), pp. 749-751.
[16] Persson P.O. Å., Hultman L., Jacobson H., Bergman J.P., Janzén E., Molina-Aldareguia J.M., Clegg W.J. and Tuomi T., Structural defects in electrically degraded 4H-SiC p+ /n / n+ diodes, Appl. Phys. Lett. 80 (2011), pp. 4852-4854.
[17] Arroyo Rojas Dasilva Y., Chauvat M.P., Ruterana P., Lahourcade L., Monroy E. and Nataf G., Defect structure in heteroepitaxial semipolar (11$\bar{2}$2) (Ga,Al)N, J. Phys.: Condens. Matter. 22 (2010), 355802.
[18] Hÿtch M.J., Putaux J.L., Pénisson and J.M., Measurement of the displacement field of dislocations to 0.03Å by electron microscopy, Nature 423 (2003), pp. 270–273.
[19] Zhao C.W., Xing Y.M., Zhou C.E. and Bai P.C., Experimental examination of displacement and strain fields in an edge dislocation core, Acta Materialia 56 (2008), pp. 2570–2575.
[20] Smeeton T.M., Kappers M.J., Barnard J.S., Vickers M.E., Humphreys C.J., Electron-beam-induced strain within InGaN quantum wells: False indium "cluster" detection in the transmission electron microscope, Appl. Phys. Lett. 83 (2003), pp. 5419-5421.
[21] Love A.E.H., Mathematical Theory of Elasticity, Cambridge University Press, Cambridge, 1927.

[22] Read W.T. Jr., Dislocations in Crystals, McGraw-Hill, London, 1953.
[23] de Wit R., Theory of disclinations: IV. Straight disclinations, J. Res. Natl. Bur. Stand. - A. Phys. and Chem. 77A (1973), pp. 607-658.
[24] Steeds J.W., Introduction to Anisotropic Elasticity Theory of Dislocations, Clarendon Press, Oxford, 1973.
[25] Dłużewski P.,Young T.D., Dimitrakopulos G. and Komninou Ph., Continuum and atomistic modelling of the mixed straight dislocation, International Journal for Multiscale Computational Engineering 8 (2010), pp. 331–342.
[26] Teodosiu C., Elastic Models of Crystal Defects, Springer-Verlag and Editura Academiei, Berlin and Bucuresti, 1982.
[27] Piela L., Ideas of Quantum Chemistry, Elsevier B.V., Amsterdam, The Netherlands, 2007.
[28] Seth B.R., Generalized strain measure with applications to physical problems, in: M. Reiner, D. Abir (Eds.), Second-Order Effects in Elasticity, Plasticity and Fluid Dynamics, Pergamon Press, Oxford, 1964, Proc. Int. Sympos., Haifa, April 23–27, 1962.
[29] Hill R., Constitutive inequalities for isotropic solids under finite strain, Proc. R. Soc. London A 314 (1970), pp. 457–472.
[30] Dłużewski P., Anisotropic hyperelasticity based upon general strain measures. Journal of Elasticity 60 (2000), pp. 119-129.
[31] Dłużewski P., Maciejewski G., Jurczak G., Kret S. and Laval J.Y., Nonlinear FE analysis of residual stresses induced by dislocations in heterostructures, Comp. Mat. Sci. 29 (2004), pp. 379–395.
[32] Kret S., P. Dłużewski and Laval J.-Y., On measurement of dislocation core distributions in GaAs/ZnTe/CdTe heterostructure by transmission electron microscopy, Phil. Mag. 83 (2003), pp. 231-244.
[33] Jain S.C., Willander M., Narayan J. and Van Overstraeten R., III-nitrides: Growth, characterization, and properties, Jpn. J. Appl. Phys. 87 (2000), pp. 965-1006.
[34] Takeuchi T., Sota S., Katsuragawa M., Komori M., Takeuchi H., Amano H. and Akasaki I., Quantum-Confined Stark Effect due to Piezoelectric Fields in GaInN Strained Quantum Wells, Jpn. J. Appl. Phys., 36 Part 2, (1997), L382.
[35] Simon J., Pelekanos N.T., Adelmann C., Martinez-Guerrero E., André R., Daudin B., Dang L.S. and Mariette H., Direct comparison of recombination dynamics in cubic and hexagonal GaN/AlN quantum dots, Phys. Rev. B 68 (2003), 035312.
[36] Rouviere P.J.L., Simon J., Pelekanos N., Daudin B. and Feuillet G., Preferential nucleation of GaN quantum dots at the edge of AlN threading dislocations, Appl. Phys. Lett. 75 (1999), pp. 2632-2634.
[37] Founta S., Bougerol C., Mariette H., Daudin B. and Vennéguès P., Anisotropic morphology of nonpolar a-plane GaN quantum dots and quantum wells, J. Appl. Phys. 102 (2007), 074304.
[38] Dimitrakopulos G.P., Kalesaki E., Kioseoglou J., Kehagias T., Lotsari A., Lahourcade L., Monroy E., Hausler I., Kirmse H., Neumann W., Jurczak G., Young T.D., Dłużewski P., Komninou P. and Karakostas T., Morphology and strain of self-assembled semipolar GaN quantum dots in $(11\bar{2}2)$ AlN, J. Appl. Phys. 108 (2010), 104304.
[39] Cherns D. and Jiao C.G., Electron Holography Studies of the Charge on Dislocations in GaN, Phys. Rev. Lett. 87 (2001), 205504.
[40] Cai J. and Ponce F.A., Determination by Electron Holography of the Electronic Charge Distribution at Threading Dislocations in Epitaxial GaN, Phys. Status Solidi A 192(2) (2002), pp. 407–411.
[41] Vurgaftman I. and Meyer J.R., Band parameters for nitrogen-containing semiconductors, J. Appl. Phys. 94 (2003), pp. 3675–3696.

[42] Taylor R.L., FEAP - A Finite Element Analysis Program, Theory Manual, University of California, Berkley, 2003, http://www.ce.berkeley.edu/projects/feap/.
[43] Jurczak G., Young T.D. and Dłużewski P., A Quantum Dot Nucleated on the Edge of a Threading Dislocation: Elastic and Electric Field Effects, Phys. Status Solidi C 10 (2013), pp. 97–100.
[44] Cholewiński J. and Dłużewski P., VECDs (Visual Editor of Crystal Defects) v. 0.4.2, software available at http://vecds.sourceforge.net.